*Supporting Information for:*

# Nitroxide-Based Macromolecular Contrast Agents with Unprecedented Transverse Relaxivity and Stability for Magnetic Resonance Imaging of Tumors

Hung V.-T. Nguyen,[†] Qixian Chen,[†] Joseph T. Paletta,[‡] Peter Harvey,[∥] Yivan Jiang,[†] Hui Zhang,[‡] Michael D. Boska,[§] M. Francesca Ottaviani,[x] Alan Jasanoff,[∥,⊥,#] Andrzej Rajca,[‡] Jeremiah A. Johnson[†,*]

[†]*Department of Chemistry,* [∥]*Department of Biological Engineering,* [⊥]*Department of Brain and Cognitive Sciences, and* [#]*Department of Nuclear Science and Engineering, Massachusetts Institute of Technology, 77 Massachusetts Avenue, Cambridge, Massachusetts 02139, United States*

[§]*Department of Radiology, University of Nebraska Medical Center, Omaha, Nebraska 68198, United States*

[x]*Department of Pure and Applied Sciences, University of Urbino, Urbino 61029, Italy*

[‡]*Department of Chemistry, University of Nebraska, Lincoln, Nebraska 68588, United States*

*Email: jaj2109@mit.edu

# Table of Contents

**Section A. Materials / General Methods / Instrumentation** **S3**

**Section B. Procedure for BASP-ORCA Synthesis** **S9**

*Representative procedure for BASP-ORCA synthesis with brush length of 7.07 and 20 equivalents of cross-linker (i.e.,* ***BASP-ORCA1****, m =7.07, N = 20)*

**Section C. Supplementary Figures** **S10**

Figure S1. Gel permeation Chromatography Traces for BASP-ORCAs S10

Figure S2. Electron Paramagnetic Resonance Spectra S11

Table S1. Nitroxide Reduction Kinetics Data Table S1 S12

Figure S3. Computational Analysis of EPR Spectra S13

Figure S4. Excitation and Emission Spectra for **BASP-ORCA1** S14

Figure S5. *In vitro* cytotoxicity of **BASP-ORCA1** S15

Figure S6. Maximum Tolerated Dose of **BASP-ORCA1** in BALB/c Mice S16

Figure S7. Pharmacokinetics and Biodistribution of **BASP-ORCA1** in BALB/c Mice S17

Figure S8. *Ex vivo* Biodistribution in Tumor-bearing Mice S18

**Section D. References** **S19**

## Section A. Materials / General Methods / Instrumentation

All reagents were purchased from commercial suppliers and used without further purification unless stated otherwise. Grubbs 3rd generation bispyridyl initiator,[1] macromonomers (MMs) **chex-MM**,[2] **Cy-MM**,[2] **PEG-MM**[3] and cross-linker **Acetal-XL**[3] were prepared according to literature procedures. Size exclusion chromatography (SEC) analyses were performed on an Agilent 1260 Infinity setup with two Shodex KD-806M columns in tandem and a 0.025 M LiBr DMF mobile phase run at 60 °C. The differential refractive index (dRI) of each compound was monitored using a Wyatt Optilab T-rEX detector, and the light scattering (LS) signal was acquired with a Wyatt Dawn Heleos-II detector. Column chromatography was carried out on silica gel 60F (EMD Millipore, 0.040–0.063 mm).

Dynamic light scattering (DLS) measurements were performed using a Wyatt Technology Mobius DLS instrument. Samples were prepared at 1.0 mg/mL in either nanopure water (MilliQ), PBS buffer, or 5% glucose solution (in nanopure water). The resulting solutions were passed through a 0.4 µm Nalgene filter (PES membrane) into disposable polystyrene cuvettes, which were pre-cleaned with compressed air. Measurements were made in sets of 10 acquisitions, and the average hydrodynamic diameters were calculated using the DLS correlation function via a regularization fitting method (Dynamics 7.4.0.72 software package from Wyatt Technology).

TEM images were acquired using a FEI Tecnai Multipurpose TEM (G2 Spirit TWIN, 12kV) at the MIT Center for Materials Science and Engineering. Samples were prepared as follows: 5 µL of a 1.0 mg/mL aqueous solution of BASP-ORCA was pipetted onto a carbon film-coated 200-mesh copper grid (Electron Microscopy Sciences) placed on a piece of parafilm. Next, the solution was carefully absorbed at the base of the droplet using the edge of a Kimwipe, leaving behind the nanoparticles on the TEM grid. The samples were then negatively stained by adding a drop of 2 wt% uranyl acetate (Electronic Microscopy Sciences). After 3 min, the residual uranyl acetate solution was carefully absorbed onto a Kimwipe, and the samples were allowed to dry completely.

Excitation/emission spectra and fluorescence measurements were acquired using a Tecan Infinite® 200 Pro plate reader. Electron Paramagnetic Resonance (EPR) spectra were acquired at the University of Nebraska using a Bruker CW X-band spectrometer equipped with a frequency counter. The spectra were obtained using a dual mode cavity; all spectra were recorded using an oscillating magnetic field perpendicular ($TE_{102}$) to the swept magnetic field. DPPH powder (g = 2.0037) was used as a g-value reference.

*Relaxivity measurements by MRI*: Phantom MRI data were acquired in a 12 cm outer diameter birdcage transceiver for imaging in a 20 cm bore Bruker 7 T Avance III MRI scanner. Samples at varying concentrations (0 up to 5 mM) in PBS buffer were loaded into the wells of a 384-well clear polystyrene plate (Thermo Scientific Nunc), which had been pre-cut in half to optimally fit the coil. Unused wells were filled with PBS buffer. 2 mm slices were imaged through the samples with the field of view of 5 x 5 cm and the data matrices were 256 x 256 points. Longitudinal ($r_1$)

and transverse ($r_2$) relaxivity measurements were acquired using multi-spin multi-echo (MSME) sequences (flip angle = 180°). $r_1$; TE = 12 ms, TR = 300, 350, 400, 450, 500, 600, 800, 1000, 1200, 1500, 3000, 5000, 10000 ms. $r_2$; TR = 5000 ms, TE = 12, 24, 36, 48, 60, 72, 84, 96, 108, 120, 132, 144, 156, 168, 280, 192, 204, 216, 228, 240, 252, 264, 276, 288, 300, 312, 324, 336, 348, 360 ms. Custom routines written in Matlab (Mathworks, Natick, MA) were used to reconstruct the images and compute relaxation time constants by fitting image intensity data to exponential decay curves.

*Kinetics of nitroxide quenching by EPR spectroscopy*: A solution was prepared with ascorbic acid (Asc), sodium phosphates (<30 ppm transition metals), sodium hydroxide and diethylenetriaminepentaacetic acid (DTPA, ~0.1% (mol/mol) to sodium phosphates) at pH 7.4. Reduced L-GSH was then dissolved to provide the Asc/GSH solution. BASP-ORCA solution was prepared in phosphate buffer, which was made from sodium phosphates and DTPA (~0.1% (mol/mol) to sodium phosphates) at pH 7.4. Equal volumes of the freshly prepared 1 mM (in nitroxide) sample solution and 20 mM Asc/GSH solution were combined and vortexed for 6 seconds, and then added to a 2 mm OD EPR tube. Kinetic studies were performed on 0.5 mM nitroxide solution in the presence of 125 mM sodium phosphates, 10 mM Asc, and 10 mM GSH. The peak height of the low-field line of the triplet was measured as a function of time. Microwave power was kept under 6.5 mW and the temperature was controlled at 295 K with a nitrogen flow system.

*Computational analysis of nitroxide quenching by EPR spectroscopy:* The EPR spectra are constituted by a "fast" and a "slow" component. From visual inspection, it was clear that the slow component was changing from one to another sample, while the fast one showed an almost equivalent line shape in the three spectra. Therefore, we first tried a computation (program by Budil and Freed[4]) of the fast component to be subtracted from the three spectra to obtain a reliable line shape for the slow components. We succeeded with the fast component shown in Figure S3A (see Section C for Figure S3A-C) (the subtracted experimental line in black and the computed line is in red). The main parameters used for the computation are shown in the figure and described below. Subtraction of this fast component from the overall spectra produced the three slow components shown in Figures S3B, S3C and S3D for 1 min, 40 min, and 180 min, respectively (in Figures S3A-S3D the spectra are normalized in height). Their computations are shown as well, together with the main parameters used for computation and analysis. The following parameters were calculated

• The $g_{ii}$ components for the coupling between the electron spin and the magnetic field (accuracy from computation ± 0.0002). The starting values, which were used in previous studies[5] using nitroxide radicals, are 2.009, 2.006, 2.003, for $g_{xx}$, $g_{yy}$, and $g_{zz}$, respectively. We found that these values worked for the computations of the fast component and for the $t$ = 1 min slow component; however, for computing the slow components of t = 40 min and 180 min it was necessary to decrease the $g_{zz}$ values to 2.0025 and 2.002, respectively. This observation indicated an increased structural anisotropy of the nitroxide labels from 1 min to 40 min to 180 min.

• The $A_{ii}$ components for the coupling between the electron spin and the nitroxide-nitrogen nuclear spin (accuracy from computation ± 0.5 G). These parameters increase with an increase in the environmental polarity of the nitroxide. Mainly, as done in previous studies,[5] the $A_{xx}$ and $A_{yy}$ values were maintained constant (6 G) and only $A_{zz}$ was changed. The polarity was found to be slightly lower for the fast component ($A_{zz}$ = 35 G) than for the slow one ($A_{zz}$ = 36 G); it was constant for the different slow components.

• The correlation time for rotational diffusion of the radical, τ (accuracy from computation ± 0.05 ns). This parameter increases with an increase in the local viscosity around the nitroxide group and with a decrease in the rotational mobility of the nitroxide. The local viscosity largely increased (the mobility decreased) from the fast component to the slow ones and it also increased (the mobility decreased) from 1 min (10 ns) to 40 min (11 ns) to 180 min (13.2 ns). Notably, by performing a subtraction procedure using the double integrals of the components of the spectra, it was found that the fast component was contained in all the three spectra in almost the same relative percentage, that is, about 20 % (the accuracy in this percentage is about 1 %).

• The line width (accuracy from computation ± 0.1 G), which measures spin-spin interactions due to a high local concentration of paramagnetic species (like colliding nitroxide groups in fast motion, or nitroxides bound in close proximity in slow motion). The line width was quite high for all samples, indicating a high local concentration of nitroxides, but it was the highest (7.6 G) for the slow component of the $t$ = 1 min sample, and it decreased at 40 min (5.5 G) and further decreased at 180 min (4.2 G). The latter value is even smaller than the line width of the fast component (4.8 G).

*Fluorimetry*: Fluorescence analysis was performed using a Tecan Infinite® 200 Pro plate reader. Absorption/emission spectra of **BASP-ORCA1** were acquired to determine $\lambda_{ex/em}$, which were 640 nm and 705 nm respectively (as expected for the dye used in these studies: Cyanine5.5). Absorption spectra were acquired using a 1 nm wavelength step size at 9 nm bandwidth; emission spectra were obtained using $\lambda_{ex}$ of 640 nm, a 5 nm wavelength step size, and 10 nm bandwidth. To examine the effect of nitroxide-quenching on fluorescence emission intensity, samples were prepared in 96-well plates (Corning, $n$ = 3) by mixing 50 µL of 5 mg **BASP-ORCA1**/mL solution with 50 µL of Asc/GSH solution with one of the following compositions: 120 equivalences (eq, with respect to **chex**) Asc, 60 eq Asc, 40 eq Asc, and 60 eq Asc + 60 eq GSH. Control samples ($n$ = 3) were prepared by mixing 50 µL of 5 mg **BASP-ORCA1**/mL solution with 50 µL of PBS. Fluorescence intensity was monitored continuously for 2 h; a plateau was typically reached within 40-50 min.

*Cell culture*: A549 and HeLa cells (ATCC) were cultured in DMEM media (Sigma-Aldrich) supplemented with 10% fetal bovine serum (FBS, VWR) and 1% penicillin/streptomycin (Thermo Fisher Scientific). Human umbilical vein endothelial cells (HUVEC, Lonza) were cultured in $EGM^+$ media (Lonza) supplemented with 1% penicillin/streptomycin. All cells were housed in 5% $CO_2$ humidified atmosphere at 37 °C.

*In vitro cell viability*: HUVEC cells were plated at 5,000 cells per well (in 100 µL) in 96-well collagen-coated plates (Corning) and allowed to adhere overnight. The media was then replaced with fresh media containing **BASP-ORCA1** at various concentrations. The plate was incubated for 72 h, and cell viability was then determined using the CellTiter-Glo assay (Promega). HeLa cells were plated in 96-well plates (Corning) and cytotoxicity was studied following the same experimental procedure used for HUVEC cells.

*Animal usage*: All experiments involving animals were reviewed and approved by the MIT Committee for Animal Care (CAC). BALB/c mice (female, 8-12 weeks old, Taconic) were used for *in vivo* toxicity, pharmacokinetic studies, and biodistribution ($n$ = 3). NCR-NU nude mice (female, 8-12 weeks old, Taconic) were used for *in vivo* MRI, NIRF imaging, and biodistribution ($n$ = 3). All animals received an alfalfa-free diet (TestDiet) at least 2 weeks prior to the start of the studies to minimize auto-fluorescence.

*In vivo toxicity*: Solutions containing 5.0–30 mg of **BASP-ORCA1** in 5% glucose were prepared, passed through sterile 0.2 µm filter (Nalgene, PES membrane), and administered into BALB/c mice via tail vein injection. The mice were monitored over a period of 30 d. Initial injections were performed in one mouse for each dose, all of which appeared to be well-tolerated. The highest dose (30 mg) was then administered to another set of mice ($n$ = 3). No adverse physical effects and/or significant weight losses were observed.

*In vivo MR and NIRF imaging instrumentation*: All imaging experiments were performed at the Koch Institute for Integrative Cancer Research at MIT. *In vivo* MRI was acquired using a Varian 7T/310/ASR-whole mouse MRI system. Scans were collected with respiratory gating (PC-SAM version 6.26 by SA Instruments Inc.) to avoid confounding noise due to chest movement. The respiratory rate and animal temperature were closely monitored during image collection. Coronal $T_2$ weighted images ($T_2$WIs) were collected using the fast spin echo multiple slices pulse sequence with $T_R$=4000 ms; $T_{E(eff)}$=48 ms; ETL=8; FOV=100×50 mm$^2$; 512×256 matrix and 2 averages over 12 slices of 1 mm thickness and 0 mm gap. Axial T2WIs were collected using the fast spin echo multiple slices pulse sequence with $T_R$=4000 ms; $T_{E(eff)}$=48 ms; ETL=8; FOV=45×45 mm$^2$; 256×256 matrix and 2 averages over 10-16 (to capture entire tumor) slices of 1 mm thickness and 0 mm gap.

*In vivo* NIRF imaging was performed on an IVIS Spectrum-bioluminescent and fluorescent imaging system (Xenogen). Epi-fluorescence imaging was acquired through excitation of the Cy5.5 fluorophore ($\lambda_{ex}/\lambda_{em}$ = 640/700 nm, exposure time 2-10s) present in **BASP-ORCA1**.

*Pharmacokinetics (PK) and biodistribution (BD) studies*: **BASP-ORCA1** doses (5.0 mg in 5% glucose) were prepared, passed through sterile 0.2 µm filters, and injected into BALB/c mice (groups of $n$ = *3*). Blood samples were taken at 1, 3, 6, 24, and 48h via cardiac puncture after euthanization in a $CO_2$ chamber. The blood samples were subjected to fluorescence imaging (IVIS, Cy5.5 $\lambda_{ex}/\lambda_{em}$ = 640/700 nm, Xenogen) for analysis of blood-compartment PK. For BD, organs

from these BALB/c mice were harvested and subjected to fluorescence imaging (IVIS, Cy5.5 $\lambda_{ex}/\lambda_{em}$ = 640/700 nm, Xenogen).

*In vivo MR and NIRF imaging in tumor-bearing mice*: A549 cells were cultured in DMEM media supplemented with 10% fetal bovine serum and 1% penicillin/streptomycin in 5% $CO_2$ humidified atmosphere (37 °C) to a final concentration of 20%. Cells were then harvested, mixed with Matrigel and sterile pH 7.4 PBS buffer (1:1), filtered through sterile 0.2 µm filters, and injected subcutaneously (2.0 x $10^6$ cells) into the hind flank of NCR-NU mice. Tumor growth was monitored for 2–4 weeks until appropriate cumulative diameters (~ 1 cm) were achieved.

MRI and NIRF images were acquired for each animal ($n$ = 3-4) before injections. **BASP-ORCA1** doses (0.16 mmol **chex**/kg or 0.23 mmol **chex**/kg in 5% glucose) were prepared, passed through a sterile 0.2 µm filter, and administered to the tumor-bearing mice via tail vein injection. Tumor imaging was done at pre-determined time points; at the last imaging time point, mice were immediately euthanized in a $CO_2$ chamber, and organs were collected, imaged by NIRF, and stored in dry ice for EPR analysis.

*Ex vivo EPR spectroscopy*: Harvested organs were shipped on dry ice to the University of Nebraska, where they were stored on dry ice. For EPR sample preparation, each tissue sample, one at a time, was rapidly thawed and transferred to a weighed vial; 900 µL of PBS buffer (0.5 mM, pH 7.2) was then added. The mixture was put into an ice-water bath and homogenized with a rotor stator homogenizer, then pipetted into a 4-mm outer diameter EPR sample tube. The samples were degassed by sonication as needed (for instance, when gas bubbles were visible). The EPR tube was capped, sealed with parafilm, and stored briefly in acetone/dry ice bath before spin concentration measurements.

Spin concentrations of nitroxide radicals in tissues (µmol **chex** per g protein; *Note:* see below for details of protein content determination) were measured at −30 °C (243.2 K) to increase signal-to-noise of the aqueous samples. Measurements of tissue samples were alternated with that of the spin concentration reference (see next paragraph) and $g$-value reference (2,2-diphenyl-1-picrylhydrazyl powder was used as the $g$-value reference). For tissue samples with low signal-to-noise, the cavity background was recorded with identical parameters, including number of scans and receiver gain. Typical parameters were as follows: microwave attenuation—20 dB, modulation amplitude—5 Gauss, spectral width—300 Gauss, resolution—512 points, conversion—40.96, time constant—10.24, and sweep time—20.97 s. These parameters were kept identical for the tissues, references, and cavity backgrounds. The number of scans (8–256) and receiver gain were adjusted as needed for each sample.

The reference for spin concentration was 0.50 mM Proxyl in PBS (pH 7.2). This reference was always stored in dry ice, except during measurements, and occasionally re-checked for spin concentration decay.

*Protein content determination*: The protein content of tissue homogenate samples was determined using the BCA Protein Assay Kit (ThermoFisher Scientific). These protein contents were then used as a normalizing parameter to compare nitroxide spin concentration and NIRF signal (Figure 6b, main text).

*Ex vivo NIRF Imaging:* To acquire BD, the collected organs and organ homogenates were subjected to NIRF imaging following the same aforementioned experimental procedure as for *in vivo* NIRF imaging. Furthermore, tissue homogenate samples were transferred into a 96-well plate and imaged for the correlation of NIRF signal and spin concentration.

*In vivo MRI data analysis:* Signal intensities pre- and post- injection were compared only using slices where tumors and muscle were clearly visible. Using ImageJ software, a region of interest (ROI) around each component was manually drawn. The average signal intensity and area of the ROI were measured; these data were then normalized against the signal intensity of the muscle tissue. Signal intensity was acquired by multiplying area and normalized signal intensity. This process was repeated for all relevant slices for a given organ; the sum of these signal intensities was then calculated and divided for the total area, affording the volume-averaged signal intensity. Signal enhancement by **BASP-ORCA1** was quantified by comparing the volume-averaged signal intensities pre- and post-injection.

*Statistical analysis:* nanoparticle diameter acquired by DLS and TEM, as well as ascorbate quenching kinetics of **BASP-ORCA1** by EPR results were reported as average ± standard deviation. *In vitro* and *in vivo* studies of **BASP-ORCA1** results were reported as mean ± standard error of the mean. Statistical comparisons were determined using student t-test where applicable.

## Section B. Procedure for BASP-ORCA Synthesis

***Note:*** *All BASP-ORCA syntheses were performed in a glovebox under $N_2$ atmosphere; however, similar results are expected under ambient conditions. All ROMP reactions followed the same general procedure, which was modified from literature examples.*[3,6]

*Representative procedure for BASP-ORCA synthesis with brush length of 7.07 (m) and 20 equivalents (N) of cross-linker (**BASP-ORCA1, m = 7.07, N = 20**):* To a 4 mL vial, a suspension of **Acetal-XL** (15.6 mg, 26.8 µmol, 20.0 eq) in THF (268.0 µL, 0.1 M **Acetal-XL**) was prepared. To a second 4 mL vial containing a stir bar, **chex-MM** (35.0 mg, 9.4 µmol, 7.0 eq) was added; **Cy-MM** was then added from a premade 12.5 mg/mL solution in THF (30.6 µL, 0.094 µmol, 0.07 eq). To a third vial, a solution of Grubbs 3rd generation bispyridyl catalyst (Grubbs III, 0.02 M in THF) was freshly prepared. THF (91.8 µL) was then added to the **MM** vial, followed by the addition of Grubbs III solution (67.0 µL, 1.3 µmol, 1.0 eq) to give the desired **MM**:Grubbs III ratio of 7.07:1 (1 mol % of the **Cy-MM**), while achieving a total **MM** concentration of **0.05 M**, affording a dark blue solution. The reaction mixture was allowed to stir for 30 min at room temperature before an aliquot (~5 µL) was taken out and quenched with 1 drop of ethyl vinyl ether for GPC analysis. The **Acetal-XL** suspension was then added dropwise (in aliquots of 5 eq, or ~70 µL, every 5 minutes) over the course of 20 min into the **MM** vial, and the polymerizing mixture was allowed to stir for 6 h at room temperature, affording a dark blue solution. To quench the polymerization, a drop of ethyl vinyl ether was added. The reaction mixture was transferred to an 8 kD molecular weight cutoff dialysis tubing (Spectrum Laboratories) in 10 mL nanopure water, and the solution was dialyzed against water (500 mL X 3, solvent exchange every 6 h). The solution of BASP-ORCA was then lyophilized to afford a blue solid.
Other BASP compositions were prepared as follows: **MM**:Grubbs III ratios of 9.99:1, 7.07:1, or 5.05:1 (*m* values). **Acetal-XL** were used in 15, 20, or 30 equivalences (*N* values). PEG-BASP, which contained no **chex**-MM, was prepared in an analogous manner to BASP-ORCAs using a PEG-MM lacking **chex**.[3] **Chex**-bottlebrush was prepared as previously described.[2]

## Section C. Supplementary Figures Cited in the Main Text

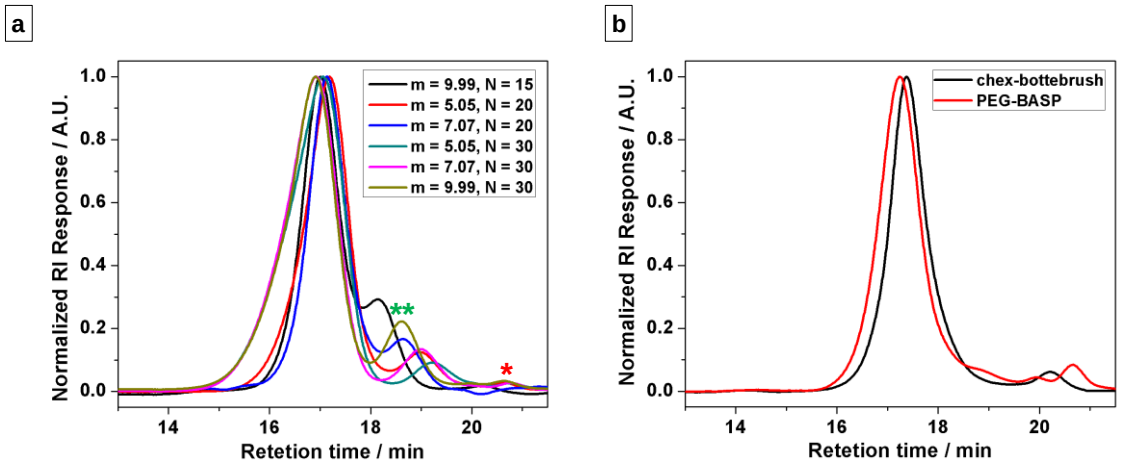


**Figure S1. a.** GPC traces of BASP-ORCAs with different brush length (*m*) and cross-linker equivalents (*N*). ***indicates negligible residual MM; **denotes uncoupled bottlebrush. In all cases, the MM-to-bottlebrush conversions were almost quantitative, while the bottlebrush-to-BASP conversions were ≥ 85%. **b.** GPC traces of **chex**-bottlebrush and PEG-BASP used for phantom MRI comparison with **BASP-ORCA1**.

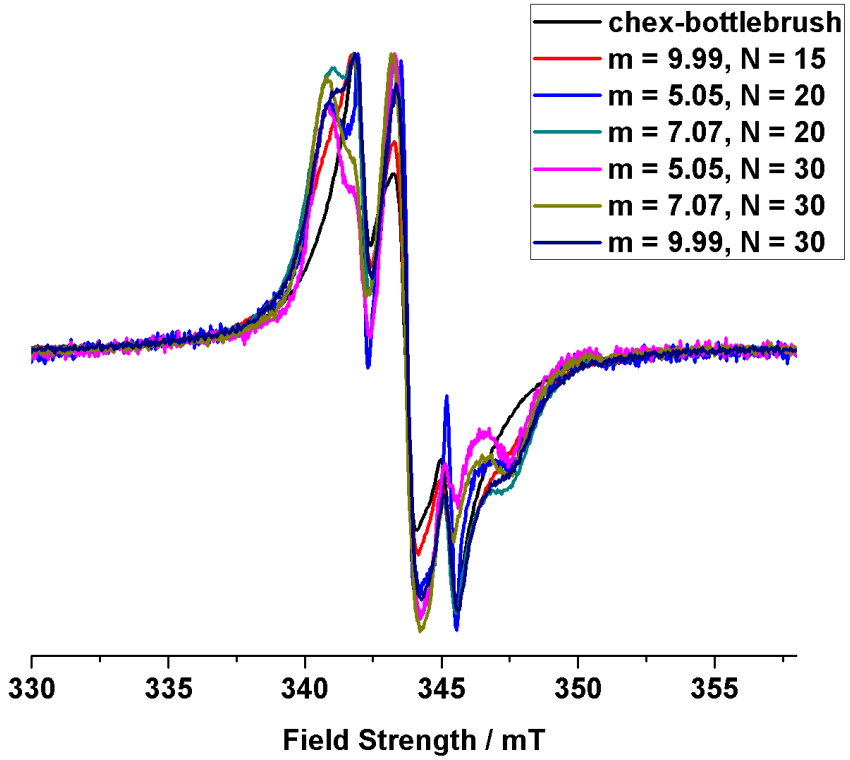


**Figure S2.** EPR spectra for BASP-ORCAs of varying composition.

## Nitroxide Reduction Kinetics:

**Table S1.** Kinetics of the reduction of nitroxides with 20-fold molar excess of ascorbate (Asc) and 0-25-fold molar excess of glutathione (GSH). Numerical fits to pseudo-first order rate equation (*k'*) peak height (PH) or integrated peak height (IPH) of the low-field EPR line.

| | | | | | | | Initial Kinetics (<1 h) | | | | | Late Kinetics (>1 h) | | | |
|---|---|---|---|---|---|---|---|---|---|---|---|---|---|---|---|
| Compd | Run No. | Run Label | Data used | Nitrox Conc. (mM) | Asc. Conc. (mM) | GSH Conc. (mM) | Range of fits | *k'* × $10^4$ ($s^{-1}$) | $R^2$ | *k* × $10^4$ ($M^{-1}s^{-1}$) | Avg *k* × $10^4$ ($M^{-1}s^{-1}$) | Range of fit (h) | *k'* × $10^4$ ($s^{-1}$) | $R^2$ | *k* × $10^4$ ($M^{-1}s^{-1}$) |
| **BASP-ORCA1**[a] | 1 | JP1191 | IPH | 0.5 | 10 | 10 | <1000 | 3.294 | 0.8795 | 329.4 | 366 ± 25 | 1.2-2.8 | 0.672 | 0.9923 | 67.2 |
| | | | IPH*[a] | | | | | 3.40 | 0.9948 | 339.7 | 334 ± 55 | | 0.586 | 0.9994 | 58.6 |
| | | | PH | | | | | 0.836 | 0.8721 | 83.6 | | | 0.297 | 0.9943 | 29.7 |
| | 2 | JP1190 | IPH | 0.5 | 10 | 10 | 115-595 | 3.712 | 0.7664 | 371.2 | | | | | |
| | | | IPH*[a] | | | | | 3.408 | 0.9910 | 340.8 | | | | | |
| | | | PH | | | | | 3.377 | 0.2923 | 33.77 | | | | | |
| | 3 | JP1189 | IPH | 0.5 | 10 | 10 | 113-613 | 3.828 | 0.7646 | 382.8 | | | | | |
| | | | IPH*[a] | | | | | 3.238 | 0.9863 | 323.7 | | | | | |
| | | | PH | | | | | 5.07 | 0.3068 | 50.7 | | | | | |
| | 4 | JP1188 | IPH | 0.5 | 10 | 10 | 126-603 | 3.818 | 0.5387 | 381.8 | | | | | |
| | | | IPH*[a] | | | | | 3.311 | 0.9938 | 331.1 | | | | | |
| | | | PH | | | | | 5.072 | 0.3366 | 50.72 | | | | | |
| | | | | | | | | | | | | | | | |
| | 1 | YW982 | IPH | 0.5 | 10 | 5.0 | 177–897 | 3.27 | 0.9633 | 327.0 | 306[b] | | | | |
| **chex**-bottlebrush | | | PH | | | | | 3.42 | 0.9702 | 342.0 | 308[b] | | | | |
| | 2 | YW983 | IPH | 0.5 | 10 | 5.0 | 396–1019 | 2.85 | 0.9520 | 285.0 | | 1.1-2.8 | 0.416 | 0.9216 | 41.6 |
| | | | PH | | | | | 2.73 | 0.9895 | 273.0 | | | 0.386 | 0.9938 | 38.6 |
| | | | | | | | | | | | | | | | |
| | 1 | YW981 | IPH | 0.5 | 10 | 0.0 | 251–851 | 3.05 | 0.9439 | 305.0 | 296[b] | | | | |
| **chex**-bottlebrush | | | PH | | | | | 2.41 | 0.9808 | 241.0 | 254[b] | | | | |
| | 2 | YW985 | IPH | 0.5 | 10 | 0.0 | 278–878 | 2.86 | 0.9145 | 286.0 | | 1.3-2.8 | 0.243 | 0.8838 | 24.3 |
| | | | PH | | | | | 2.68 | 0.9775 | 268.0 | | | 0.196 | 0.9735 | 19.6 |
| | | | | | | | | | | | | | | | |
| **chex**-dendrimer[7] | 1 | JP609 | IPH | 0.5 | 10 | 0.0 | 90-390 | 6.20 | 0.6609 | 620.0 | 603 ± 123 | 0.8-2.8 | 0.301 | 0.6847 | 30.1 |
| | | | PH | | | | | 6.17 | 0.9718 | 617.0 | 579 ± 59.6 | | 0.354 | 0.9663 | 35.4 |
| | 2 | JP610 | IPH | 0.5 | 10 | 0.0 | 115-415 | 7.18 | 0.6743 | 718.0 | | | | | |
| | | | PH | | | | | 6.09 | 0.9336 | 609.0 | | | | | |
| | 3 | JP611 | IPH | 0.5 | 10 | 0.0 | 126-426 | 4.72 | 0.7984 | 472.0 | | | | | |
| | | | PH | | | | | 5.10 | 0.9915 | 510.0 | | | | | |
| | | | | | | | | | | | | | | | |
| **3-CP**[8] | 1 | JP899 | IPH | 0.2 | 4.0 | 5.0 | <600 | 2.435 | 0.9997 | 608.8 | 608.0 ± 4.2 | | | | |
| | | | PH | | | | | 2.361 | 0.9990 | 590.3 | 602.6 ± 25 | | | | |
| | 2 | JP8100 | IPH | 0.2 | 4.0 | 5.0 | <600 | 2.438 | 0.9997 | 609.6 | | | | | |
| | | | PH | | | | | 2.410 | 0.9996 | 602.4 | | | | | |
| | 3 | JP1101 | IPH | 0.2 | 4.0 | 5.0 | <600 | 2.423 | 0.9998 | 605.6 | | | | | |
| | | | PH | | | | | 2.461 | 0.9996 | 615.2 | | | | | |
| | | | | | | | | | | | | | | | |
| **3-CP**[7,9] | 1 | JP460 | IPH | 0.2 | 4.0 | 0.0 | <3600 | 2.547 | 0.9996 | 636.8 | 625 ± 22 | | | | |
| | | | PH | | | | | 2.504 | 0.9949 | 636.0 | 611 ± 44 | | | | |
| | 2 | JP461 | IPH | 0.2 | 4.0 | 0.0 | <3600 | 2.498 | 0.9975 | 624.5 | | | | | |
| | | | PH | | | | | 2.396 | 0.9949 | 599.0 | | | | | |
| | 3 | JP462 | IPH | 0.2 | 4.0 | 0.0 | <3600 | 2.459 | 0.9999 | 614.8 | | | | | |
| | | | PH | | | | | 2.389 | 0.9961 | 597.3 | | >1 | 1.18 | 0.9952 | 295 |
| | | | | | | | | | | | | | | | |

[a] For **BASP-ORCA1**, double integration of entire EPR spectra gave initial rate constant $k = 449 \pm 23$ $M^{-1}s^{-1}$, which is somewhat larger than the integrated peak height (IPH) value, $k = 366 \pm 25$ $M^{-1}s^{-1}$; IPH* is the integrated peak height for the center line of the EPR spectrum. [b] For ORCA-Fluor, initial second order rate constants from 4 kinetic runs using 0 – 10 equiv of GSH, $k = 301 \pm 20$ and $281 \pm 43$ $M^{-1}s^{-1}$ for baseline corrected IPH and PH data. Data for **chex**-bottlebrush,[2] data for **chex**-dendrimer (baseline corrected) and late kinetics for **3-CP** with Asc only,[7] data for **3-CP** with 20 equiv of Asc and 25 equiv of GSH,[8] and data for **3-CP** with Asc only[9] were reported elsewhere); the reported values represent the mean and standard deviation (*n = 2-4*).

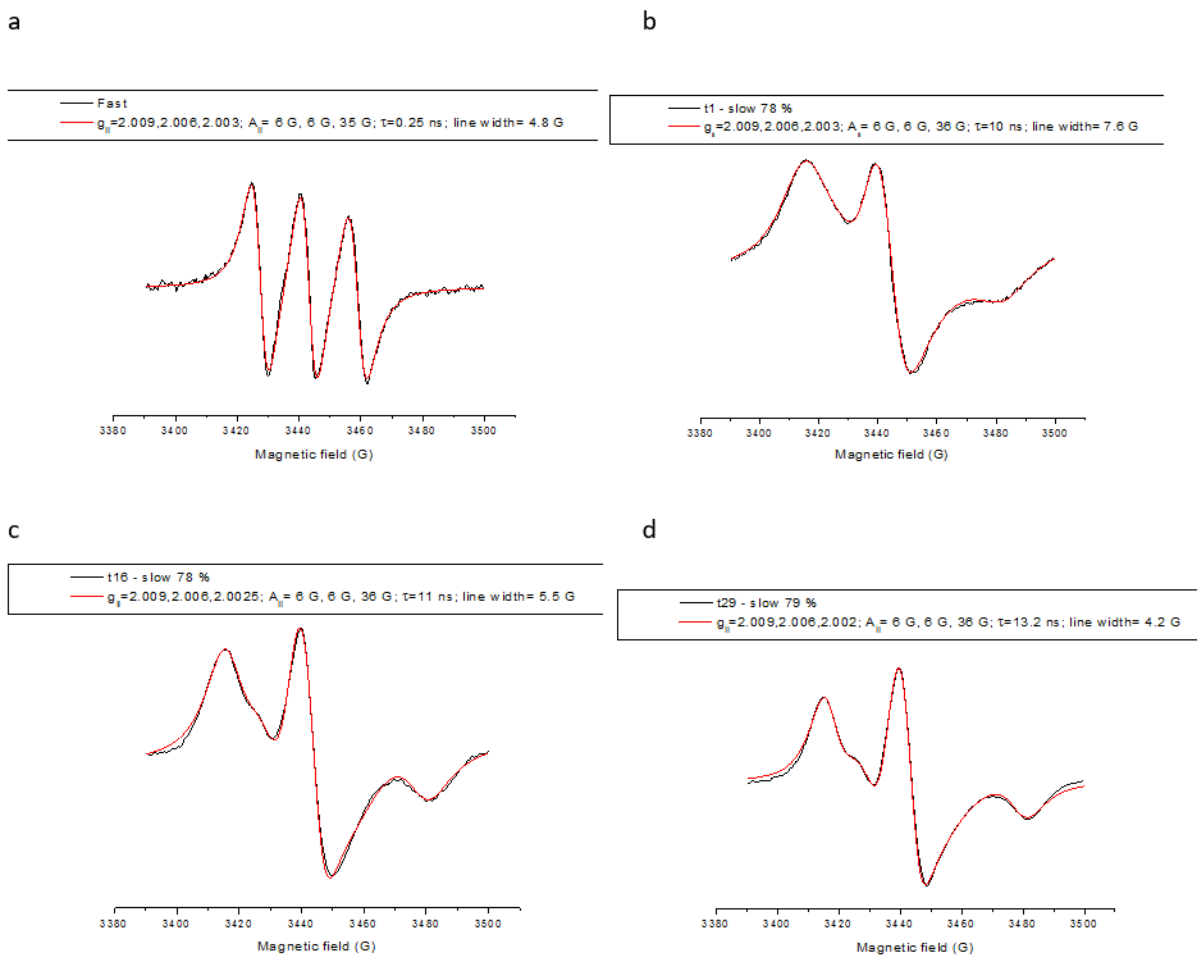


**Figure S3.** Computational analysis of EPR spectra obtained during reduction kinetics experiments: **a.** fast component **b.** t1 = 1 min **c.** t16 = 40 min and **d.** t29 = 180 min of slow component following addition of Asc solution.

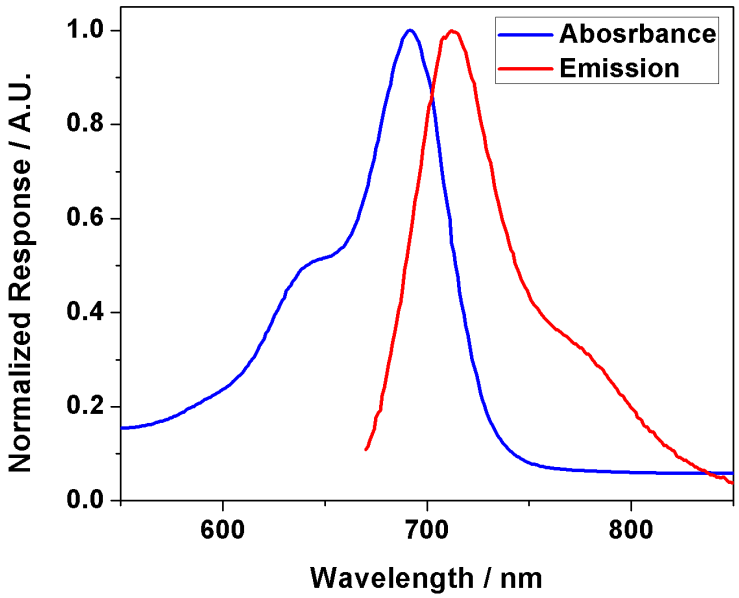


**Figure S4.** Excitation and emission spectra of **BASP-ORCA1**.

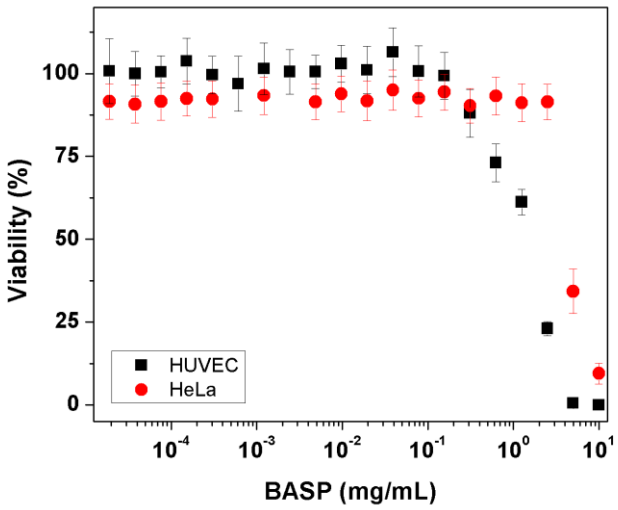


**Figure S5.** Cell viability assay for **BASP-ORCA1** in the toxin-sensitive HUVEC and cancerous HeLa cell lines as measured by CellTiter Glo. No toxicity was observed until high concentrations were reached (up to 0.3 mg/mL and 5 mg/mL for HUVEC and HeLa, respectively); the reported values represent the mean and standard error of the mean (*n* = *4*).

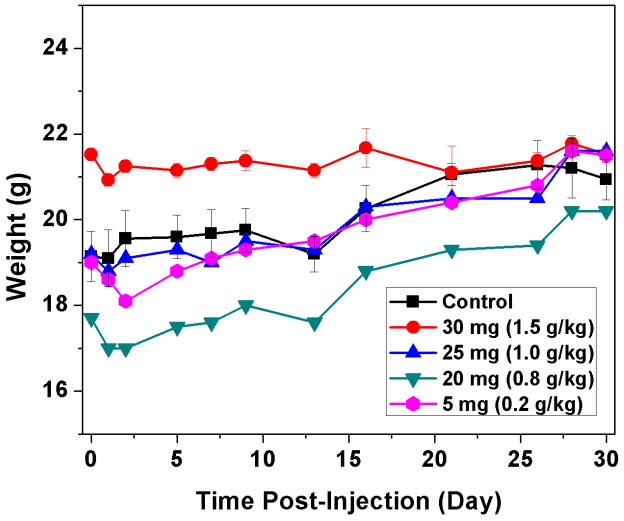


**Figure S6.** *In vivo* gross toxicity of **BASP-ORCA1** following intravenous injections in BALB/c mice; the reported values represent the mean and standard error of the mean. The control and highest dose experiments were performed with $n$ = 3, whereas lower doses were done with $n$ = 1.

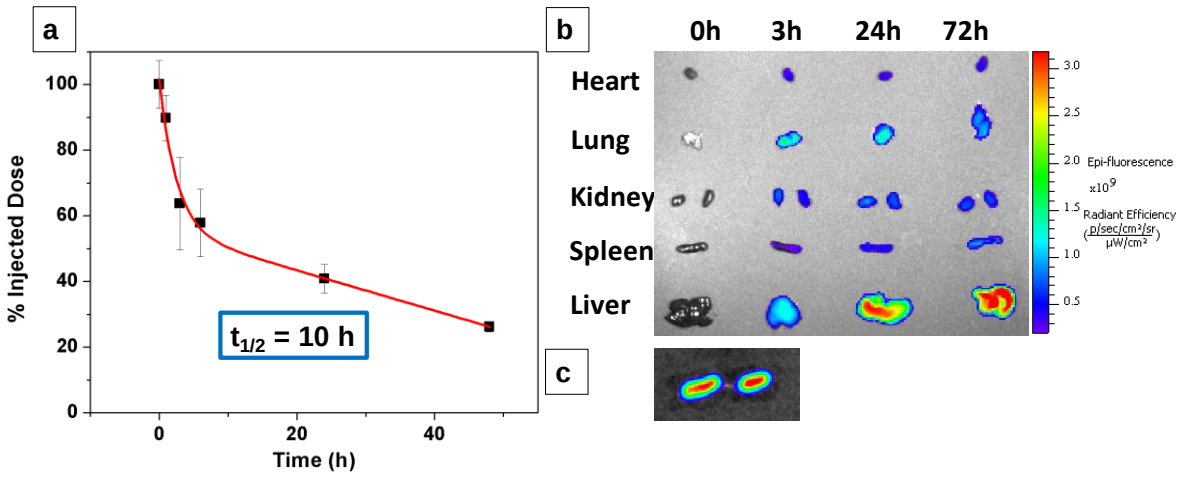


**Figure S7.** **a.** Pharmacokinetics (PK), **b.** biodistribution (BD), and **c.** excrements collected 24 h after administration of **BASP-ORCA1** in BALB/c mice as imaged by NIRF ($\lambda_{ex}/\lambda_{em}$ = 640/700 nm). PK data were fit into a two-component model using standard procedures ($R^2$ = 0.95).[2,5] The reported values represent the mean and standard error of the mean (*n = 3*).

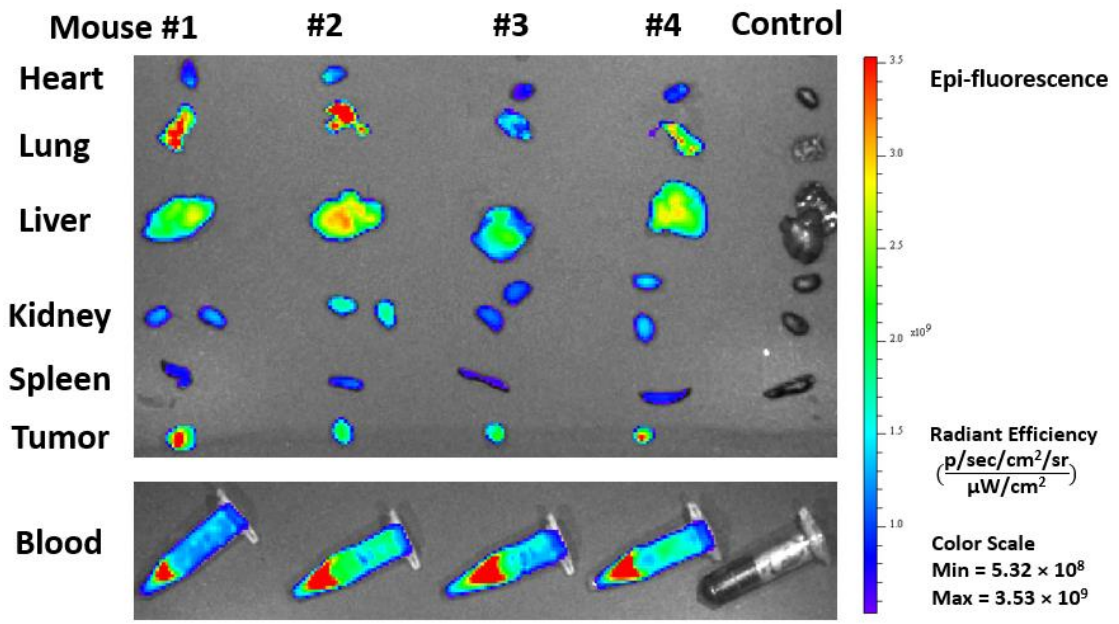


**Figure S8.** *Ex vivo* BD as assessed by NIRF imaging ($\lambda_{ex}/\lambda_{em}$ = 640/700 nm) of subcutaneous tumor-bearing NCR-NU mice following injection of **BASP-ORCA1**. Experiments were done with $n$ = 4.

## Section D. References


[1] Love, J. A.; Morgan, J. P.; Trnka, T. M.; Grubbs, R. H. A Practical and Highly Active Ruthenium-based Catalyst that Effects the Cross Metathesis of Acrylonitrile. *Angew. Chem. Int. Ed.* **2002**, *41*, 4035–4037.

[2] Sowers, M. A.; McCombs, J. R.; Wang, Y.; Paletta, J. T.; Morton, S. W.; Dreaden, E. C.; Boska, M. D.; Ottaviani, M. F.; Hammond, P. T.; Rajca, A.; Johnson, J. A. Redox-Responsive Branched-bottlebrush Polymers for *in vivo* MRI and Fluorescence Imaging. *Nat. Commun*. **2014**, *5*, 5460.

[3] Gao, A. X.; Liao, L.; Johnson, J. A. Synthesis of Acid-Labile PEG and PEG-doxorubicin-conjugate Nanoparticles via Brush-first ROMP. *ACS Macro Lett*. **2014**, *3,* 854–857.

[4] Budil, D. E.; Lee, S.; Saxena, S.; Freed, J. H. Nonlinear-least-square Analysis of Slow-motion EPR Spectra in One and Two Dimensions Using a Modified Levenberg-Marquardt-algorithm. *J. Magn. Reson., Ser. A*. **1996**, *120*, 155-189

[5] Angelov, V.; Velichkova, H.; Ivanov, E.; Kotsilkova, R.; Delville, M-H.; Cangiotti, M.; Fattori, A.; Ottaviani, M. F. EPR and Rheological Study of Hybrid Interfaces in Gold-clay-epoxy Nanocomposites. *Langmuir.* **2014**, *30*, 13411-13421.

[6] Liao, L.; Liu, J.; Dreaden, E. C.; Morton, S. W.; Shopsowitz, K. E.; Hammond, P. T.; Johnson, J. A. A Convergent Synthetic Platform for Single-nanoparticle Combination Cancer Therapy: Ratiometric Loading and Controlled Release of Cisplatin, Doxorubicin, and Camptothecin. *J. Am. Chem. Soc*. **2014**, *136*, 5896–5899.

[7] Rajca, A.; Wang, Y.; Boska, M.; Paletta, J. T.; Olankitwanit, A.; Swanson, M. A.; Mitchell, D. G.; Eaton, S. S.; Eaton, G. R.; Rajca, S. Organic Radical Contrast Agents for Magnetic Resonance Imaging. *J. Am. Chem. Soc.* **2012**, *134*, 15724-15727.

[8] Wang, Y.; Paletta, J. T.; Berg, K.; Reinhart, E.; Rajca, S.; Rajca, A. Synthesis of Unnatural Amino Acids Functionalized with Sterically Shielded Pyrroline Nitroxides. *Org. Lett.* **2014**, *16*, 5298–5300.

[9] Paletta, J. T.; Pink, M.; Foley, B.; Rajca, S.; Rajca, A. Synthesis and Reduction Kinetics of Sterically Shielded Pyrrolidine Nitroxides. *Org. Lett.* **2012**, *14*, 5322-5325.